Journal of Instrumentation

PAPER

Optimization of detector placements in reduction of multiple counts for μSR measurements at China Spallation Neutron Source

To cite this article: Jingyu Dong *et al* 2022 *JINST* **17** P01017

Published by IOP Publishing for Sissa Medialab

Received: *October 8, 2021*
Accepted: *December 22, 2021*
Published: *January 12, 2022*

Optimization of detector placements in reduction of multiple counts for μSR measurements at China Spallation Neutron Source

Jingyu Dong,[a] **Ziwen Pan,**[a,*] **Zebin Lin,**[a] **Zhe Wang,**[a] **Zhengyang He,**[a] **Jiandang Liu,**[a] **Hongjun Zhang,**[a] **Hantao Jing,**[b,c] **Yu Bao,**[b,c] **Jingyu Tang**[b,c] **and Bangjiao Ye**[a,*]

[a] *State Key Laboratory of Particle Detection and Electronics, University of Science and Technology of China, Hefei 230026, China*
[b] *Institute of High Energy Physics, Chinese Academy of Sciences (CAS), Beijing 10049, China*
[c] *Spallation Neutron Source Science Center (SNSSC), Dongguan 523803, China*

E-mail: panzw19@ustc.edu.cn, bjye@ustc.edu.cn

Abstract: An Experimental Muon Source (EMuS) has been proposed to conduct muon spin rotation/relaxation/resonance (μSR) measurements at China Spallation Neutron Source (CSNS). To make better use of muons in each pulse, a highly segmented μSR spectrometer with more than 2000 detector channels is under design. Due to such high granularity of detectors, multiple counting events generated from particle scattering or spiral motion of positrons in a strong longitudinal field should be carefully considered in the design. According to the simulation, long scintillators have a good capability of angular discrimination. Detectors with cuboid geometries are better than those with frustum shapes. The cuboid detector with a length of 50 mm is longer enough to get the optimal range of discrimination angle. In a real μSR spectrometer, detectors can be placed parallelly along the beam direction or pointing to the sample. A figure of merit (FoM) has been proposed to compare such two arrangements by integrating their impacts on multiple counts and total counting loss in zero and longitudinal fields. The outstanding performance of multiple counting rejection due to the angular discrimination capability makes the pointing arrangement achieve much higher FoM. The simulation results can provide good support for the design of the highly segmented μSR spectrometer.

Keywords: Muon spectrometers; Detector modelling and simulations I (interaction of radiation with matter, interaction of photons with matter, interaction of hadrons with matter, etc); Simulation methods and programs

*Corresponding author.

https://doi.org/10.1088/1748-0221/17/01/P01017

2022 JINST 17 P01017

Contents

2022 JINST 17 P01017

1 Introduction

Muon is an leptonic particle with a spin of 1/2. High energetic particles (protons or heavy ions) can generate pions by bombarding on a pion production target. Subsequently, pions decay into muons and muon neutrinos with a lifetime of 26 ns. In the coordinate of the pion, the spin and the momentum of muons are anti-parallel to keep the momentum conservation. By collecting muons with a small angular dispersion, their average polarization is up to 100%. Muons will decay into positrons with a lifetime of $\sim$ 2.2 µs. According to the violation of parity conservation in weak interaction, positrons emit asymmetrically in space and preferentially along the muon spin. The muon spin can precess in the local magnetic field inside the materials. As a result, the asymmetrical distribution of decay positrons will change in correlation with the magnetic property of materials. Detection of the asymmetry by placing detectors in the forward and backward directions of a sample forms the basis of the μSR (muon spin rotation/relaxation/resonance) techniques.

The μSR spectrometer is the key instrument in muon facilities [1–5] to dissolve magnetic information inside materials. The precision of μSR data directly depends on the counting rate and the intrinsic asymmetry of the spectrometer. In pulsed μSR experiments, positrons generated in each pulse are almost detected by the spectrometer without relating back to their individual parental muons [3–5]. Consequently, it is possible that the spectrometer records some multiple counts in each pulse. Three types of multiple counting events can be detected by the spectrometer, mimicking good positron events: 1) a positron penetrates several detectors by scattering or spiral motion in a strong magnetic field, 2) secondary particles like electrons or gamma rays generated by positrons or muons, 3) positrons decay from muons but outside the sample. In terms of the first two situations, both positrons and their induced secondaries carry the same asymmetry information with their parental muons. Therefore, the detection of the asymmetry by the spectrometer cannot be affected. However, it will increase the statistical error of the measured data [6]. For the last case, the real information of internal magnetic fields inside a sample will be blurred by its surrounding materials (sample chamber, collimator, beam pipe, etc.) [7].

The Experimental Muon Source (EMuS) has been proposed to be constructed at Phase II of China Spallation Neutron Source (CSNS) [8]. About 5% of the proton beam power (500 kW, 1.6 GeV, 25 Hz) will be assigned to EMuS. The μSR spectrometer is under design [9–11]. In

order to achieve higher counting rate, several thousand detector segments have been considered in the spectrometer design. As a result, the measuring time can be greatly shortened. However, the fraction of multiple counts will increase due to the high granularity. Hence, a capability of angular discrimination for multiple counts is needed in the design of μSR detectors. The placement of detectors determines the total covered solid angle which influences the total counting rate and the intrinsic asymmetry of the spectrometer. As over 99% positrons have the energy higher than 10 MeV, they can easily penetrate small plastic scintillators. The pathlength of charged particles inside detectors depends on their emission angle and detector placement. The energy deposition of these particles is positively correlated with the pathlength. Therefore, it is possible to discriminate charged particles within a given range of emission angle by selecting their energy deposition and optimizing the detector placement. For μSR experiments, the angle and the kinetic energy of decay positrons and their induced multiple counts are different when penetrating plastic scintillators. A better placement of detectors can help reject multiple counts by taking advantage of the angular discrimination capability described above. In this work, Monte Carlo simulations based on musrSim [12] have been done to optimize the placement of detectors in the design of a highly segmented μSR spectrometer for EMuS.

2 Energy deposition response of a single detector

For charged particles, the energy deposition is nearly proportional to the pathlength when penetrating a scintillation detector. The pathlength of positrons inside a long scintillator varies with the incident angle, so it is possible to discriminate positrons in a selected angular range. As illustrated in figure 1, the energy deposition of positrons hitting a cuboid or frustum detector (frustum of a pyramid) with varied angle θ is simulated by Geant4 [13–15]. The kinetic energy of positrons is set the same with those decayed from muons, which can be expressed as

$$N(\varepsilon) = 2\varepsilon^2(3 - 2\varepsilon) \tag{2.1}$$

where N is the positron counts and ε is the kinetic energy of positrons relative to the maximum value (52.8 MeV). Figure 1 shows the dimensions of two detector geometries. The width of both detectors is 10 mm. The length of detector changes from 10 to 100 mm.

Figure 2 shows the average energy deposition of positrons varying the incident angle θ. For detectors with a length of 20 to 100 mm for the two geometries, when the incident angle θ is 0, the pathlength of positrons is the longest and the average energy deposition is the highest. When the incident angle θ gradually increases to 90 degrees, the pathlength of positrons decreases monotonously, so does the average energy deposition. In the case of the cuboid detector with a length of 10 mm, the pathlength of positrons oscillates when rotating the detector. As a result, the average energy deposition shows an oscillation trend. For the frustum detector with a length of 10 mm, the pathlength of positrons is the shortest with θ of 0 and longest with θ of 90°.

Except for detectors with a length of 10 mm, the average energy deposition presents a similar downturn trend as a function of θ. As the incident angle increases, the average pathlength of positrons penetrating the detector decreases, resulting in a decrease of average deposition energy. The monotonic decreasing trend as shown in figure 2 indicates that it is possible to record positrons within a narrow range of incident angle. To be more exact, a long detector can help discriminate multiple

2022 JINST 17 P01017

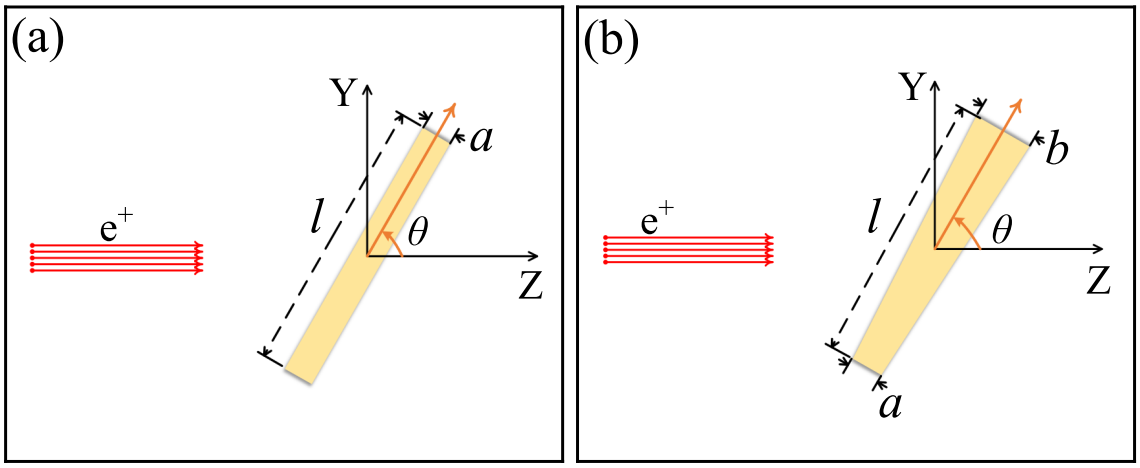

Figure 1. Schematic diagram of positrons incident on (a) a cuboid detector and (b) a frustum detector (frustum of a pyramid) in variation with the incident angle θ. The plastic scintillation material is EJ200. The width a is fixed to 10 mm, l is the length, and b equals to $0.4l$+10 mm which keeps the ratio $(b-a)/l$ with a constant value of 0.4.

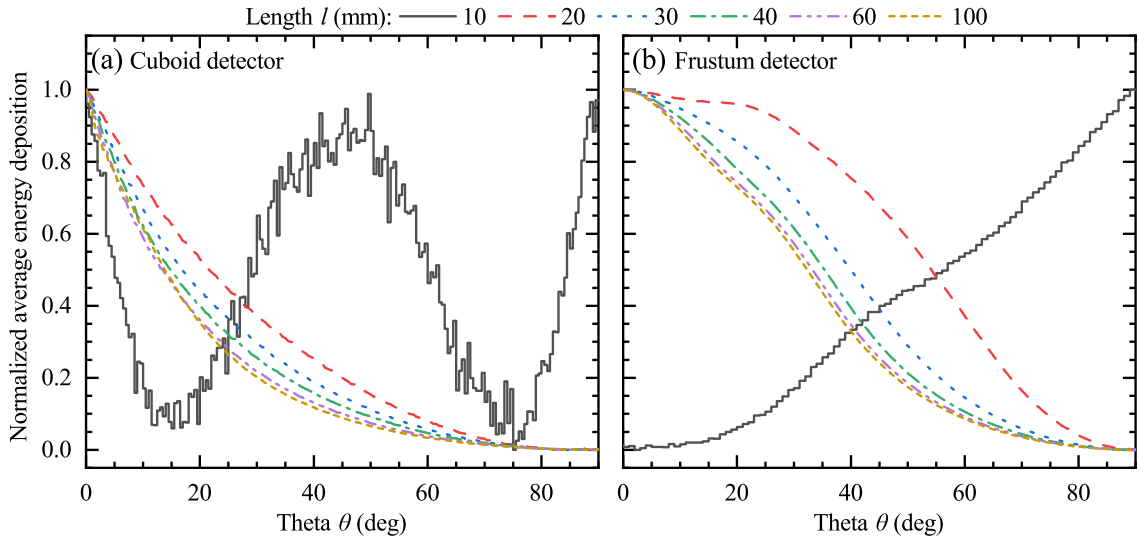

Figure 2. Angular dependence of average energy deposition for (a) the cuboid detector and (b) the frustum detector.

counts in real μSR measurements. In comparison of two detector geometries, the distribution of the average energy deposition with incident angle is narrower for the cuboid detector.

According to the simulation results in figure 2, the angular discrimination range in a given energy threshold is used to quantitatively compare the angular discrimination capability of two detector geometries. Detectors taking up a narrow discrimination range can more effectively eliminate influences of multiple counts. Figure 3 shows the angular discrimination range as a function of the detector length varying the energy threshold. For any given energy threshold, the angular discrimination range of the cuboid detector is narrower than that of the frustum detector. It also

2022 JINST 17 P01017

indicates that setting a higher energy threshold can improve the angular discrimination capability but result in a loss of positron counts. A longer detector has a narrower angular discrimination range which tends to be stable for the detector length over 40 mm. The downturn trend in figure 3 presents an exponential decrease correlated with the detector length, which can be expressed as

$$\gamma = Ae^{-\frac{l}{\lambda}} + B \tag{2.2}$$

where γ is the angular discrimination range, B is the base range, and A is the width of the range. A narrow range of $(B, A + B)$ indicates a better angular discrimination capability for a detector. A detector with a small λ means it can effectively discriminate multiple counts with a relatively short length. Accordingly, the angular discrimination capability can be estimated by

$$C = \frac{1}{B\int_0^\infty Ae^{-\frac{l}{\lambda}}\mathrm{d}l} = \frac{1}{BA\lambda} \tag{2.3}$$

where C represents the capability of angular discrimination for a detector. The influences of parameters A, B and λ are integrally considered in eq. (2.3).

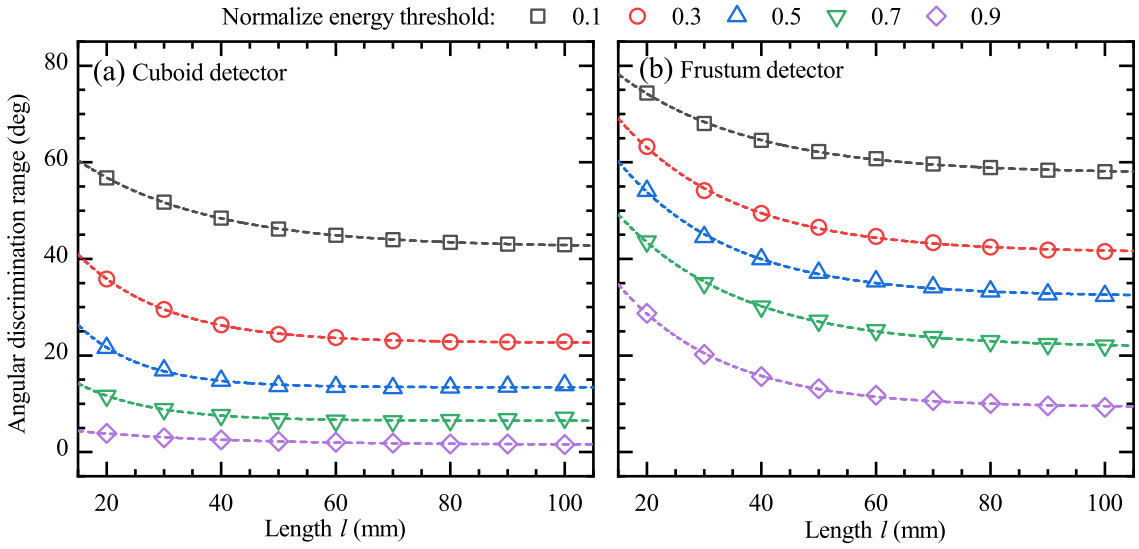

Figure 3. Angular discrimination range extracted from figure 2. All dashed curves are fitted from the data points. Note that cases with any other thresholds in the range (0, 1) share similar exponential reduction trends as shown in the plot.

Figure 4(a) shows the results of the angular discrimination capability with respect to the energy threshold. Values of the capability for both detector geometries present a rising trend as a function of the energy threshold. The cuboid detector has a relatively higher angular discrimination capability compared with that of the frustum detector. Such two conclusions drawn from figure 4(a) agree well with the simulation results in figure 2. It confirms the feasibility of eq. (2.3). Therefore, the cuboid detector is a better choice for the design of a μSR spectrometer. According to the fitted λ shown in figure 4(b), a detector with a length of 50 mm (2λ) is longer enough to achieve the angular discrimination range of 7 degrees according the restriction set for spectrometers at RIKEN-RAL [16].

2022 JINST 17 P01017

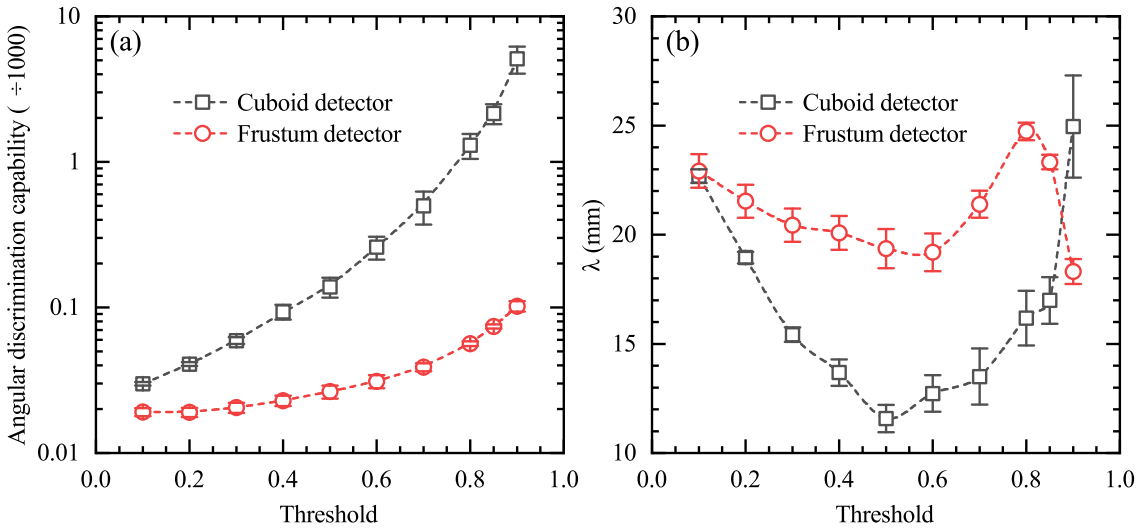

Figure 4. (a) Angular discrimination capability and (b) fitting parameter λ for two detector geometries in variation with the energy threshold.

3 Impact of multiple counts on a real detector ring

For pulsed μSR spectrometers, parallel [17–19] and pointing [20, 21] arrangements are always selected to place detector arrays as shown in figure 5. Scattered positrons or secondary particles may cause multiple counts as shown in figure 5. According to the simulation in section 2, long scintillators have a good capability of angular discrimination due to the difference of pathlength or energy deposition when particles penetrate the detector from different directions. In the case of the parallel arrangement, the advantage of angular discrimination in long scintillators have not been played out. Positrons emitted in the angular range (θ_1, θ_2) can be recorded by the detection system, resulting in a wide distribution of acceptable energy deposition. Therefore, multiple counts with similar energy deposition can also be accepted by the detectors. In the case of the pointing arrangement, positrons decayed from the sample can penetrate the longest path inside a detector. The successful usage of the angular discrimination capability in such detector placement can help the detection system suppress the multiple counts with relatively low energy deposition.

A longitudinal field ranging from 0 to several tesla is usually added in the sample environment of μSR experiments. As positrons are charged particles, they can do spiral motion under strong magnetic field. It is possible that more than two detectors can be fired by the same position on its spiral trajectory as shown in figure 6(a). Figure 6(b) shows the percentage of multiple counts for two types of detector arrangements varying the longitudinal field from 0 to 10 T. For the parallel arrangement, the percentage of multiple counts increases from around 0 to 3% below 0.5 T which is in the similar range of MUSR at ISIS [17]. Thereafter, the percentage shows a rapid rise in strong fields (over 1 T) and reaches ~ 50% which is much higher than the current acceptable value (~ 30% in simulation) from the running experience of HiFi [17, 19, 22]. Due to the spiral motion of charged particles, the counting rate varies in correlation with the field. Hence, a "valley" occurs in the up-down trend. The variation of multiple counts in the pointing arrangement also presents an up-down trend. The

2022 JINST 17 P01017

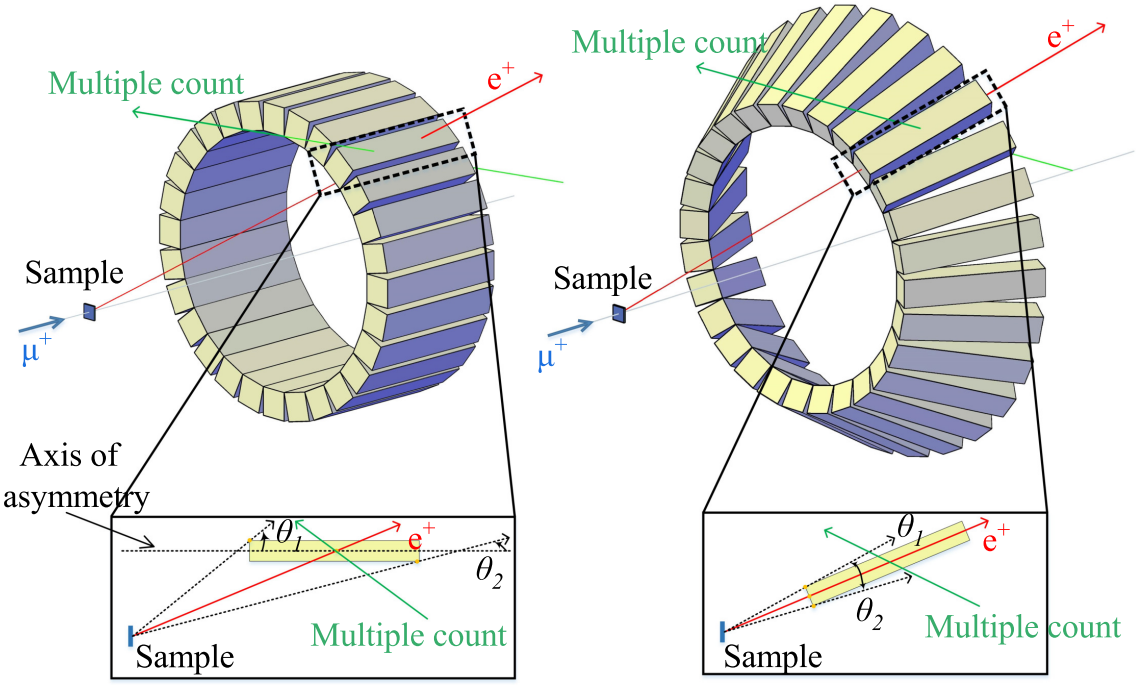

Figure 5. (a) Parallel and (b) pointing arrangement of μSR detector rings. Note that θ_1 and θ_2 are the angles between position tracks and the symmetrical axis of a positron detector.

percentage is lower than ~ 5% which benefits from the good angular discrimination capability of long scintillators pointed to the sample. Figure 6(c) shows the counting losses of two arrangements relative to those in a zero field. The two arrangements present different trends. Owing to the spiral motion of charged particles in the strong longitudinal field, the angular distribution of positrons emitted from the sample is suppressed, which presents a more preferential direction along the beam direction. In the parallel arrangement, detectors cover a relatively large solid angle with respect to the beam direction. Furthermore, such detector placement can accept all positrons whose energy deposition exceed the threshold. Therefore, the positron count in figure 6(c) shows an increasing trend below ~ 3.5 T, and then reduces to ~ 0 at 10 T. For the pointing arrangement, positrons can not perpendicularly hit its detectors. As these detectors select positrons within a narrow range of hitting angle, the total positron counts present a reduction trend if a longitudinal field is performed. According to the analysis above, the percentage of multiple counts and the counting loss show a competitive relation. To estimate the total impacts of such two parameters, a figure of merit is proposed as

$$\mathrm{FoM} = \frac{1 - C_{\mathrm{loss}}}{M^2} \tag{3.1}$$

where C_{loss} denotes the counting loss, and M is the percentage of multiple counts. Figure 6(d) shows the FoM for two arrangements. The FoM of both arrangements present a downturn trend. The pointing arrangement can achieve a much higher FoM than that of the parallel arrangement, especially in the range of (0, 1) T. The quick reduction of FoM for the pointing arrangement indicates that more detector rings should be added to get a higher counting rate.

2022 JINST 17 P01017

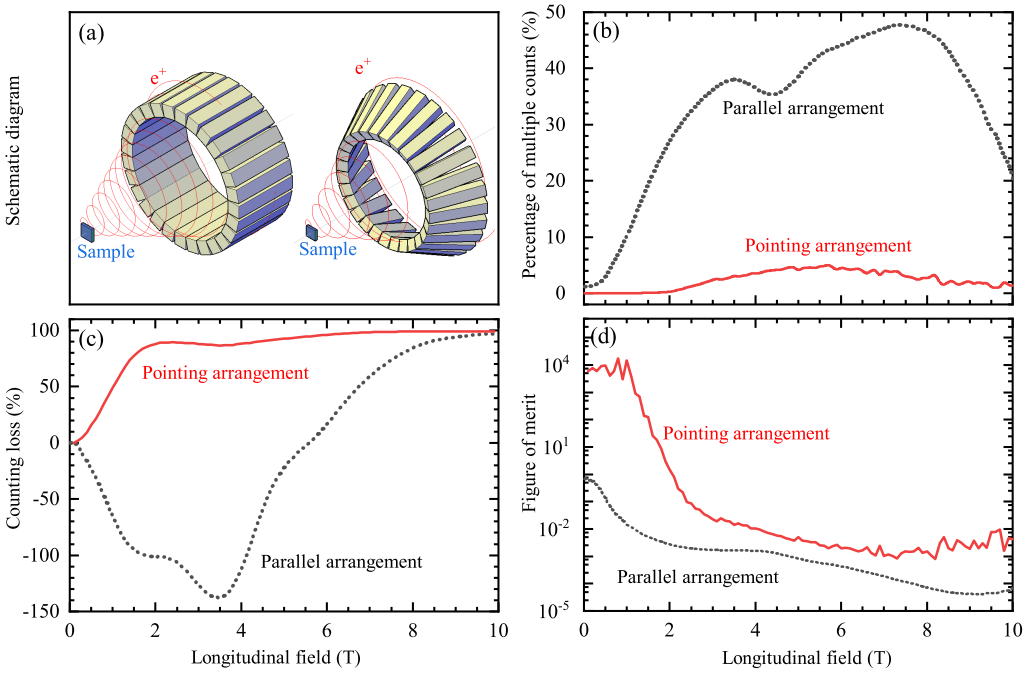

Figure 6. (a) Schematic view of multiple counts, (b) percentage of multiple counts, (c) counting loss (negative value means counting increase) and (d) figure of merit in a longitudinal field.

4 Conclusions

In this work, the impacts of detector geometry and placement on multiple counts have been studied by using Monte Carlo simulations. It is confirmed that long scintillators have better capability of angular discrimination by varying the hitting angle of positron beam onto a detector in simulations. The angular discrimination capability regarding the angular discrimination range and characteristic length of a detector has been proposed to quantitatively estimate the performance of multiple counting rejection for different detector geometries. Compared with frustum detectors, cuboid detectors have a better angular discrimination capability. Such cuboid geometry with a length of 50 mm is longer enough to get the optimal range of angular discrimination. Thereafter, two detector arrangements consisting of parallel and pointing placements in zero and longitudinal fields were carefully studied. A figure of merit has been proposed to take into integrated consideration the percentage of multiple counts and counting loss in zero and longitudinal fields. By taking advantage of the angular discrimination capability of long scintillators, the pointing arrangement performs much better than the parallel arrangement, especially in the field below 1 T. For the pointing arrangement, its figure of merit reduced quickly as a function of the field owing to the counting loss in strong fields. Therefore, more detector rings should be added to a spectrometer to get more positron counts.

2022 JINST 17 P01017

Acknowledgments

This work was supported by National Natural Science Foundation of China (Grant No. 12005221). We are very grateful for the STFC ISIS Muon Group and Detector Group, especially Adrian Hillier for his useful comments and valuable suggestions.

References

[1] R. Abela et al., *The μSR facilities at PSI*, *Hyperfine Interact.* **87** (1994) 1105.

[2] J.L. Beveridge, J. Doornbos and D.M. Garner, *Muon facilities at TRIUMF*, *Hyperfine Interact.* **32** (1986) 907.

[3] G.H. Eaton, *The ISIS pulsed muon facility*, *Z. Phys. C* **56** (1992) S232.

[4] Y. Miyake et al., *J-PARC muon source, MUSE*, *Nucl. Instrum. Meth. A.* **600** (2009) 22.

[5] A. Yamamoto et al., *MuSIC, the world's highest intensity DC muon beam using a pion capture system*, *Conf. Proc. C.* **110904** (2011) 820.

[6] J.S. Lord et al., *Design and commissioning of a high magnetic field muon spin relaxation spectrometer at the ISIS pulsed neutron and muon source*, *Rev. Sci. Instrum.* **82** (2011) 073904.

[7] M. Lynch, S. Cottrell, P. King and G. Eaton, *Measuring small samples at the ISIS muon source*, *Physica B* **326** (2003) 270.

[8] J. Tang et al., *EMuS muon facility and its application in the study of magnetism*, *Quantum Beam Sci.* **2** (2018) 23.

[9] X.J. Ni et al., *Design and test of μSR detection system of EMuS at CSNS*, 2019 *JINST* **14** T04004.

[10] Z.-W. Pan et al., *Conceptual design and update of the* 128*-channel μSR prototype spectrometer based on musrSim*, *Nucl. Sci. Tech.* **30** (2019) 123.

[11] Z. Pan et al., *Development of L-bent positron detectors for μSR applications at china spallation neutron source*, *IEEE Trans. Nucl. Sci.* **68** (2021) 2407.

[12] K. Sedlak, R. Scheuermann, T. Shiroka, A. Stoykov, A. Raselli and A. Amato, *MusrSim and MusrSimAna — simulation tools for μSR instruments*, *Phys. Procedia* **30** (2012) 61.

[13] GEANT4 collaboration, *GEANT*4 *— a simulation toolkit*, *Nucl. Instrum. Meth. A* **506** (2003) 250.

[14] J. Allison et al., *GEANT*4 *developments and applications*, *IEEE Trans. Nucl. Sci.* **53** (2006) 270.

[15] J. Allison et al., *Recent developments in GEANT*4, *Nucl. Instrum. Meth. A* **835** (2016) 186.

[16] D. Tomono et al., *Development of new μ-e decay counter in new multi-channel μSR spectrometer for intense pulsed muon beam*, *Nucl. Instrum. Meth. A* **600** (2009) 44.

[17] R.J. da S. Afonso et al., *Monte Carlo simulations of the μSR spectrometer at ISIS: current instrument and future designs*, *RAL Tech. Rep.* (2015) 1.

[18] S.R. Giblin et al., *Optimising a muon spectrometer for measurements at the ISIS pulsed muon source*, *Nucl. Instrum. Meth. A* **751** (2014) 70 [arXiv:1404.4542].

[19] Z. Salman et al., *HiFi — a new high field muon spectrometer at ISIS*, *Physica B* **404** (2009) 978.

[20] R. Kadono et al., *Development of a new μSR spectrometer ARGUS*, *RIKEN Accel. Prog. Rep.* **29** (1996) 196.

[21] D. Tomono et al., *Progress in development of new μSR spectrometer at RIKEN-RAL*, *J. Phys. Conf. Ser.* **225** (2010) 012056.

[22] J.S. Lord et al., *Design and commissioning of a high magnetic field muon spin relaxation spectrometer at the ISIS pulsed neutron and muon source*, *Rev. Sci. Instrum.* **82** (2011) 073904.

2022 JINST 17 P01017